

Atomic Dark Matter

David E. Kaplan* Gordan Z. Krnjaic† Keith R. Rehermann‡ Christopher M. Wells§

*Department of Physics and Astronomy
Johns Hopkins University
3400 North Charles Street
Baltimore, MD 21218-2686*

September 3, 2009

Abstract

We propose that dark matter is dominantly comprised of atomic bound states. We build a simple model and map the parameter space that results in the early universe formation of hydrogen-like dark atoms. We find that atomic dark matter has interesting implications for cosmology as well as direct detection: Protohalo formation can be suppressed below $M_{proto} \sim 10^3 - 10^6 M_\odot$ for weak scale dark matter due to Ion-Radiation interactions in the dark sector. Moreover, weak-scale dark atoms can accommodate hyperfine splittings of order 100 keV, consistent with the inelastic dark matter interpretation of the DAMA data while naturally evading direct detection bounds.

1 Introduction

Cosmological observations suggest that dark matter comprises more than 80% of the matter in the universe [1, 2]. Much of the effort to explain the origin of dark matter has focused on minimal solutions in which dark matter consists of a single particle species, the most popular being the neutralino in variants of the supersymmetric standard model. Such dark matter models include the compelling feature that weak-scale physics – weak-scale mass and weak-force coupling strength – can naturally generate dark matter with the correct cosmological abundance. Dark matter in this broad class is described as weakly interacting massive particles (WIMPs).

However, conflicts do exist between WIMP models and observational data. Simulations of WIMP dark matter predict significantly more small-scale structure than current observations suggest [3, 4]. In addition, the direct detection experiment, DAMA [5], sees a positive signal with great significance (8σ), yet when interpreted as a standard WIMP, other experiments such as CDMS [6] and XENON10 [7], completely rule out the same parameter space. Finally, measured cosmic ray spectra may suggest a new primary source for electrons and positrons in our galaxy and potentially evidence for dark-matter annihilation; however,

*dkaplan@pha.jhu.edu

†gordan@pha.jhu.edu

‡keith@pha.jhu.edu

§cwells13@pha.jhu.edu

the standard neutralino candidate is unable to fit this data [8, 9, 10, 11].

These issues suggests compelling reasons to explore dark matter models beyond the minimal candidate. In addition, the dark matter sector (or ‘dark sector’) may be rich with complexity and may feature unanticipated dynamics. In fact, the dark matter may even interact via a long-range force – a massless gauge boson – which is still allowed by the bounds on the number of relativistic degrees of freedom during big bang nucleosynthesis [12].

In this paper we propose a dark sector charged under a hidden U(1) gauge symmetry. We assume two species of fermions, a ‘dark proton’ and a ‘dark electron’, and that the dark matter abundance comes from a matter–anti-matter asymmetry.¹ We shall see that in interesting parts of parameter space, the bulk of the dark matter exists in atomic bound states. The Lagrangian is

$$\mathcal{L}_{dark} = \bar{\Psi}_{\mathbf{p}}(\mathcal{D} + m_{\mathbf{p}})\Psi_{\mathbf{p}} + \bar{\Psi}_{\mathbf{e}}(\mathcal{D} + m_{\mathbf{e}})\Psi_{\mathbf{e}} \quad (1)$$

where $\mathcal{D} = i\partial + gQ\mathcal{A}$ and $Q = \pm 1$ for $\Psi_{\mathbf{p}}$ and $\Psi_{\mathbf{e}}$ respectively. In what follows we use the convention $m_{\mathbf{p}} \geq m_{\mathbf{e}}$ without loss of generality. We show (Section 2) that for parts of parameter space, recombination in the dark sector occurs efficiently, and we discuss the bounds from and implications for structure formation. We then add interactions which allow for direct detection in a way that mimics inelastic dark matter [15] and show that there exist parts of parameter space which can explain the DAMA signal, while avoiding constraints from other direct detection experiments (Section 3). Finally, in Section 4 we discuss, in a cursory way, other phenomena potentially related to atomic dark matter.

A number of ideas related to this work have appeared in the literature. For example, the idea of U(1) charged dark matter has appeared in [16, 17], the idea of composite dark matter in [18], and that of mirror dark matter in [19, 20]. To our knowledge, this is the first work to explore the generic parameter space for viable atomic dark matter.

2 Cosmology

Introducing a new hidden U(1) has interesting cosmological implications. Our interests lie in the parameter space that affords atomic systems. The existence of standard model (SM) atomic hydrogen states in the early universe requires an asymmetry between particles and antiparticles; dark atoms are no different. We assume that there is a ‘dark asymmetry’ akin to the baryon asymmetry in the SM, and that the dark asymmetry is such that the universe is net charge neutral, $n_{\mathbf{e}} = n_{\mathbf{p}}$.² The existence of dark atoms implies that dark matter is coupled to dark radiation until the universe cools beyond the binding energy of hydrogen

$$B = \frac{1}{2}\alpha_D^2\mu_{\mathbf{H}}, \quad (2)$$

where α_D is the dark fine structure constant and $\mu_{\mathbf{H}} = (m_{\mathbf{e}}m_{\mathbf{p}})/(m_{\mathbf{e}} + m_{\mathbf{p}})$ is the reduced mass of dark hydrogen. This has potentially interesting implications for structure formation because interactions in the

¹ Some models that use the matter–anti-matter asymmetry to generate the correct dark matter abundance exist [13, 14], but we do not explore them here.

²Unless otherwise noted, \mathbf{e} , \mathbf{p} , and \mathbf{H} refer to the dark electron, dark proton, and dark hydrogen, respectively.

dark sector can decouple much later than in a conventional CDM WIMP model. Observations of satellite galaxies seem to favor some mechanism to damp the growth of small scale structure in dark matter [21, 22], which, as discussed below, can be provided by atomic dark matter.

2.1 Dark Recombination and Halo Constraints

One of the most interesting features of the model is the presence of both neutral and ionized dark matter components. The fractional ionization, X_e , plays an important role in the cosmic evolution of the dark matter. At early times, X_e affects the decoupling temperature of dark matter and dark radiation, which impacts small-scale structure formation of dark matter. At late times, bounds on dark matter self-interactions constrain X_e because the dark matter ions interact through a long range force. The residual ionization fraction in the dark sector is governed by neutral atom formation in analogy with SM hydrogen recombination [23]. In the following, we follow the notation of Ref. [24].

The residual ionization fraction is found by solving the Boltzmann equation for the free dark electron fraction,

$$X_e \equiv \frac{n_e}{n_e + n_H}. \quad (3)$$

The evolution of X_e depends on the Hubble rate, H , and the rate for $\mathbf{e} + \mathbf{p} \leftrightarrow \mathbf{H} + \gamma$. We can write the thermally-averaged recombination cross section using the dimensionless variable $x = \frac{B}{T}$ as

$$\langle \sigma v \rangle = \xi \frac{64\pi}{\sqrt{27}\pi} \frac{\alpha_D^2}{\mu_H^2} x^{1/2} \ln(x). \quad (4)$$

where $\xi = 0.448$ is a best-fit numerical coefficient [25, 26]. The equation governing X_e can be written as

$$\frac{dX_e}{dx} = C \frac{1}{Hx} \left[(1 - X_e)^2 \beta - X_e^2 n_{DM} \langle \sigma v \rangle \right] \quad (5)$$

where

$$\beta = \langle \sigma v \rangle \left(\frac{B m_e}{2\pi x} \right)^{3/2} e^{-x}. \quad (6)$$

As discussed in [23, 25], recombination into the $n = 2$ state completely dominates the evolution of X_e . This is accounted for through the factor C in Eq. (5) which represents the fraction of $n = 2$ states that produce a net gain in the number of ground state hydrogen atoms. This is not unity because the thermal bath can ionize the $n = 2$ state before it decays. Thus, C is the ratio of the ($n = 2 \rightarrow n = 1$) decay rate to the sum of this decay rate plus the ionization rate (see [23] for a detailed discussion)

$$C = \frac{\Lambda_\alpha + \Lambda_{2\gamma}}{\Lambda_\alpha + \Lambda_{2\gamma} + \beta^{(2)}}. \quad (7)$$

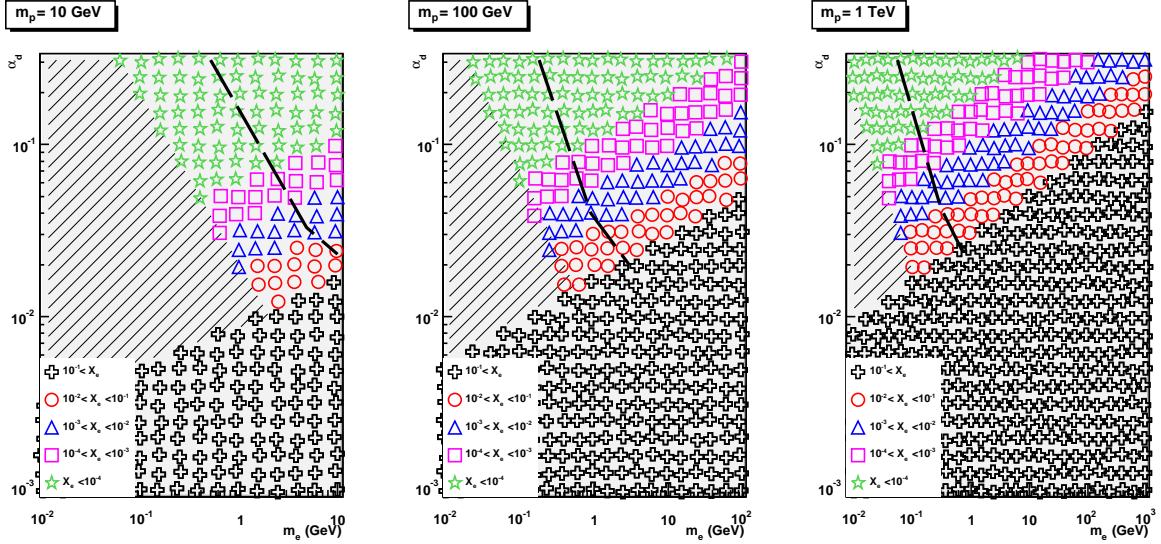


Figure 1: The allowed parameter space in $\alpha_D - m_e$ for a given m_p and as a function of the residual ionization fraction, X_e . Atom dark matter is viable in the colored regions, which correspond to $10^{-2} < X_e < 10^{-1}$ (red circles), $10^{-3} < X_e < 10^{-2}$ (blue triangles), $10^{-4} < X_e < 10^{-3}$ (magenta boxes) and $X_e < 10^{-4}$ (green stars). The striped region is ruled out by Eq. 21 with $\kappa = 3$ and this region extends to the dashed black line for $\kappa = 10$. The black-crossed region is ruled out because $X_e > 10\%$.

The rates are given by

$$\beta^{(2)} = \beta e^{3x/4} \quad (8)$$

$$\Lambda_\alpha = H \frac{(3B)^3}{(8\pi)^2} \frac{1}{(1 - X_e) n_{DM}} \quad (9)$$

$$\Lambda_{2\gamma} = 3.8 \frac{3^2}{2^{11}} \frac{\alpha^8 \mu_H}{4\pi} \quad (10)$$

where Λ_α the rate for a Lyman- α photon to redshift such that it cannot excite $n = 1 \rightarrow n = 2$ and $\Lambda_{2\gamma}$ is the two photon decay rate of $2s \rightarrow 1s$, which has been taken from Ref. [27]. We find that X_e varies from $1 - 10^{-10}$ throughout the parameter space $\alpha_D \in [10^{-3}, 0.3]$, $m_e \in [0.01 \text{ GeV}, m_p]$, $m_p \in [m_e, 3 \text{ TeV}]$. Self-interactions, as discussed below, rule out some of this parameter space. A few representative planes are plotted in Figure 1.

Bounds on the atomic parameter space and X_e can be derived from observations of the Bullet Cluster and halo profiles. The bounds are derived through the momentum transfer cross section³

$$\sigma_{mt}^i = \int d\Omega (1 - \cos \theta) \frac{d\sigma^i}{d\Omega} \quad (11)$$

³Note that σ_{mt} reduces to the total elastic cross section for hard-sphere s-wave scattering which is typical of WIMP dark matter models.

where the index i runs over the three types of self-interactions present in our dark sector: Hydrogen–Hydrogen, Ion–Hydrogen, and Ion–Ion. The last process is described by Coulomb scattering, but since we want to study a dominantly atomic dark sector, the Ion–Ion cross section is the least relevant to our model and we do not discuss it further. Naïvely, the first two cross sections are bounded by geometric values

$$\frac{d\sigma}{d\Omega} \leq a_0^2, \quad (12)$$

where $a_0 = 1/(\alpha \mu_{\mathbf{H}})$ is the Bohr radius of dark hydrogen. However, this naïve guess is inadequate. At low energies ($ka_0 \ll 1$) both of these processes can be described by scattering from a central potential

$$V \propto r^{-n} \quad (13)$$

with $n = 6$ and 4 , respectively. In this case one finds that the cross sections are velocity-independent constants and enhanced over the geometric estimate [28]. We are generally interested in a wide range of ka_0 , thus these results are not strictly applicable however these cross sections are slowly decreasing functions of the relative velocity [28]. A conservative estimate of the cross sections is given by

$$\frac{d\sigma}{d\Omega} \leq (\kappa a_0)^2, \quad (14)$$

with $3 \leq \kappa \leq 10$. The values of κ have been inferred from general quantum mechanical scattering [29, 30] and detailed computations of SM hydrogen scattering [31, 32, 33].

With the relevant cross sections in hand, we can use observations of the Bullet Cluster [34, 35] as a guide for the present day maximum value of $X_{\mathbf{e}}$. Measurements of the mass-to-light ratio and the radius of the sub-cluster suggest that the sub-cluster could have lost no more than $F_{obs} = 20 - 30\%$ of its initial mass. Following the analysis in [34], the number of scattering centers that a single dark matter particle encounters as it passes through the target cluster in the case of one species is

$$\tau = \frac{\sigma}{m} \Xi_s; \quad (15)$$

this quantity is often referred to as the scattering depth. The parameter Ξ_s is the surface mass density of the sub-cluster defined as

$$\Xi_s \equiv \int_0^R \rho(z) dz, \quad (16)$$

where $\rho(z)$ is the sub-cluster’s volume mass density and R is the radius of the sub-cluster. For multiple species, with species i in the sub-cluster having a mass density Ξ_i , and mass m_i , scattering off of species j in the target cluster, we have

$$\tau_{ij} = \left(\frac{\Xi}{m} \right)_i \sigma_{ij} f_j \quad (\text{no sum}) \quad (17)$$

where σ_{ij} is the cross section for i and j to interact and f_j is the number fraction of species j in the target cluster. Equation 17 can be rewritten in terms of total observed surface mass density, $\Xi_T = \sum_i \Xi_i$, as

$$\tau_{ij} = \Xi_T \frac{f_i}{\sum_k f_k m_k} \sigma_{ij} f_j. \quad (18)$$

We make the simplifying and conservative assumption that all of the ions in the sub-cluster are scattered out of the sub-cluster. In this case, the mass fraction lost through $H - j$ scattering is bounded by

$$F_{\mathbf{H}} = F_{obs} - f_{\mathbf{p}} \frac{m_{\mathbf{p}}}{m_{\mathbf{H}}} - f_{\mathbf{e}} \frac{m_{\mathbf{e}}}{m_{\mathbf{H}}} = F_{obs} - X_{\mathbf{e}}. \quad (19)$$

The mass fraction actually lost from the sub-cluster, using cross sections as parameterized in (14) and (18), is

$$\Delta = \sum_j \tau_{Hj} = \frac{\Xi_T}{m_{\mathbf{H}}} (1 - X_{\mathbf{e}}^2) 4\pi \kappa^2 a_0^2. \quad (20)$$

Demanding that $\Delta < F_{\mathbf{H}}$ we have the bound

$$\frac{\sigma}{m_{\mathbf{H}}} = \kappa^2 \frac{a_0^2}{m_{\mathbf{H}}} < \frac{F_{obs} - X_{\mathbf{e}}}{\Xi_T (1 - X_{\mathbf{e}}^2)}. \quad (21)$$

Plugging in the values $\Xi_T = 0.2 - 0.3 \text{ cm}^{-2} \text{ g}$ and $F_{obs} = 0.2$ gives a constraint on the atomic parameter space [34]

$$\left(\frac{0.1}{\alpha_D}\right)^2 \left(\frac{1 \text{ GeV}}{\mu_{\mathbf{H}}}\right)^2 \left(\frac{100 \text{ GeV}}{m_{\mathbf{H}}}\right) \lesssim (20 - 200) \frac{0.2 - X_{\mathbf{e}}}{1 - X_{\mathbf{e}}^2}. \quad (22)$$

Thus, we find that $X_{\mathbf{e}}$ and $\sigma/m_{\mathbf{H}}$ are bounded simultaneously. From our conservative (and representative) assumption about the Ion-Ion cross section, $X_{\mathbf{e}}$ is bounded to be less than 10% – 20% regardless of $\sigma/m_{\mathbf{H}}$. For very small $X_{\mathbf{e}}$, the usual CDM WIMP bounds on $\sigma/m_{\mathbf{H}}$ are applicable; our estimate yields $\sigma/m_{\mathbf{H}} \lesssim 1 \text{ cm}^2/\text{g}$, which is slightly larger than the detailed simulations of [35]. Figure 1 shows some of the allowed parameter space in the $\alpha_D - m_{\mathbf{e}}$ plane for a few atomic masses ranging between 10 GeV and 1 TeV.

Previous considerations of a hidden $U(1)$ [16, 17] have concluded that soft scattering of charged dark matter can drastically affect halo formation and thereby rule out large swaths of parameter space. This result follows from the soft singularity in the Rutherford scattering rate which, when integrated over galactic time scales, can lead to significant energy transfer between charged particles. This effect tends to smooth out the core of the dark matter distribution. Application of these results excludes *all* of the parameter space shown in Figure 1. However, since Hydrogen-Hydrogen scattering is well modelled by hard-sphere scattering in the majority of the considered parameter space, these bounds are not applicable to atomic dark matter. The relevant bounds from halo formation considerations are $0.1 \text{ cm}^2/\text{g} \lesssim \sigma/m_{\mathbf{e}} \lesssim 1 \text{ cm}^2/\text{g}$, which do not significantly change our conclusions [36]. Atomic dark matter provides a dynamical mechanism to shut off the naïve long range effects of a hidden $U(1)$.

2.2 Protohalos and Radiation Damping

Certain values of the residual ionization fraction may enable the ionized dark matter to smooth out structure on small scales. The parameter space of atomic dark matter allowed by constraints derived in Section 2.1 predict that kinetic decoupling of the dark matter fluid and dark radiation occurs during the radiation dominated epoch. The dark radiation damps the growth of structure until it decouples from the dark matter [37]. The decoupling temperature is given by

$$\Gamma(T_{dec}) = H(T_{dec}) \quad (23)$$

where

$$\Gamma(T) = n_e \sigma_T = X_e n_{DM} \sigma_T \quad (24)$$

$$H(T) = \frac{5}{3} \sqrt{g_*} \frac{T^2}{M_{pl}} \simeq 5.5 \frac{T^2}{M_{pl}} \quad (25)$$

and σ_T is the Thomson cross section, $\sigma_T = 8/3\pi(\alpha_D/m_e)^2$. Using (23) - (25) the decoupling temperature is given by⁴

$$T_{dec} \simeq 10 \left(\frac{0.1}{\alpha_D}\right)^2 \left(\frac{0.1}{X_e}\right) \left(\frac{m_e}{1 \text{ GeV}}\right)^2 \left(\frac{m_H}{100 \text{ GeV}}\right) \text{ keV}. \quad (26)$$

A full analysis of the power spectrum is left to future work (see [16, 37, 38] for discussions of similar effects), however, a rough estimate of the comoving wavenumber that is damped due to the radiation interaction is

$$k_{damp} \lesssim \frac{1}{\eta_{dec}} \quad (27)$$

where η_{dec} is the conformal time of decoupling. This can be written in terms of today's temperature, T_0 , and the decoupling temperature T_{dec}

$$\eta_{dec} = 2t_{dec}(1 + z_{dec}) \simeq \frac{M_{pl}}{T_0 T_{dec}}. \quad (28)$$

The mass scale which survives damping, and which eventually characterizes the first dark matter clumps, can be written as

$$\begin{aligned} M_{grow} &> \frac{4\pi}{3} \left(\frac{\pi}{k_{damp}}\right)^3 \Omega_{DM} \rho_{crit} \\ &\gtrsim (10^3 - 10^6) \left(\frac{T_{dec}}{10 \text{ keV}}\right)^{-3} M_\odot \end{aligned} \quad (29)$$

where ρ_{crit} is today's value and the largest value of M_{grow} corresponds to $k_{dec} = \eta_{dec}^{-1}$. The large range of M_{grow} occurs because we have allowed for an order of magnitude error in k_{dec} . Thus, we find that atomic dark matter can have much less power on small scales compared to a conventional CDM WIMP if there is a sizeable fraction of free electrons. In particular, weak-scale dark atoms can be consistent with the observed populations of intermediate mass dark halos in the Milky Way [4]. We emphasize that simulations are necessary to evaluate the detailed power spectrum and satellite populations predicted by atomic dark matter. However, it is clear that even the simplest atomic dark matter system can significantly impact structure formation.

⁴Most of the allowed parameter space requires $B < \Lambda_{QCD}$, thus we take $g_* = 12$.

3 Direct Detection

Atomic dark matter, as thus far considered, is secluded from the standard model. While the cosmology of atomic dark matter is interesting in its own right, it naturally lends itself to inelastic scattering because of energy level quantization. This offers an exciting possible explanation of the DAMA data [5].

The unperturbed energy levels of hydrogen are

$$E_n = \frac{\alpha_D^2 \mu_{\mathbf{H}}}{2n^2}. \quad (30)$$

One might hope that the DAMA scale – $\mathcal{O}(100 \text{ keV})$ – could be generated by energy differences between levels with different principle quantum numbers. Generically the rate of elastic scattering will be greater than that of inelastic scattering. However, predominantly inelastic scattering could be enforced by setting $m_{\mathbf{p}} = m_{\mathbf{e}} = 2\mu_{\mathbf{H}}$. In this case, the first Born term for elastic scattering vanishes. Unfortunately, efficient recombination in such a scenario forces one to consider $m_{\mathbf{H}} \sim \text{GeV}$, which is too small to account for the recoil energies measured by DAMA. Nevertheless, atoms have a rich structure and the allowed parameter space for viable recombination naturally leads to *hyperfine splittings* on the order of 100 keV for weak-scale hydrogen. The hyperfine splitting is given by

$$E_{hf} = \frac{2}{3} g_{\mathbf{e}} g_{\mathbf{p}} \alpha_D^4 \mu_{\mathbf{H}} \frac{m_{\mathbf{e}}}{m_{\mathbf{p}}} \quad (31)$$

where $g_{\mathbf{e}}, g_{\mathbf{p}}$ are the gyromagnetic ratios of the dark electron and dark proton, which we take to be equal to two.

Exploiting this scale requires a scattering process which is dependent on the spins of the dark atom's constituents. This can be accomplished with a broken $U(1)_X$ which is axially coupled to the dark matter and mixed with the standard model hypercharge as in [18]

$$\mathcal{L}_{mix} = \epsilon X^{\mu\nu} B_{\mu\nu}. \quad (32)$$

Having an axial coupling in the dark sector and a vector coupling to the standard model will ensure that the dominant scattering process changes the dark atom spin state by one unit. After integrating out the Z boson and diagonalizing the gauge kinetic terms, the Lagrangian is

$$\begin{aligned} \mathcal{L} &= \mathcal{L}_{SM} + \mathcal{L}_{DM} + \mathcal{L}_{Dark\ Gauge} \\ \mathcal{L}_{DM} &= \bar{\Psi}_{\mathbf{p}}(i\partial - g_5 \gamma_5 \mathcal{X} + g\mathcal{A} + m_{\mathbf{p}})\Psi_{\mathbf{p}} + \bar{\Psi}_{\mathbf{e}}(i\partial + g_5 \gamma_5 \mathcal{X} - g\mathcal{A} + m_{\mathbf{e}})\Psi_{\mathbf{e}} - \frac{\epsilon s_w}{m_Z^2} J_{Z\mu} J_D^\mu \\ \mathcal{L}_{Dark\ Gauge} &= -\frac{1}{4} A_{\mu\nu}^2 - \frac{1}{4} X_{\mu\nu}^2 - \left(\epsilon c_w J_{EM}^\mu + \epsilon s_w \left(\frac{M_X}{m_Z} \right)^2 J_Z^\mu \right) X_\mu + \frac{M_X^2}{2} X^2. \end{aligned} \quad (33)$$

The parameters c_w and s_w are the cosine and sine of the weak mixing angle. The dark current J_D^μ is

$$J_D^\mu = -g_5 \bar{\Psi}_{\mathbf{p}} \gamma^\mu \gamma_5 \Psi_{\mathbf{p}} + g_5 \bar{\Psi}_{\mathbf{e}} \gamma^\mu \gamma_5 \Psi_{\mathbf{e}}, \quad (34)$$

and J_{EM}^μ and J_Z^μ are the standard model electromagnetic and weak neutral currents, respectively.

The calculation of the direct detection scattering cross section is organized as follows. First, we derive the non-relativistic interaction Hamiltonian for dark atoms and standard model nucleons from Eq. (33). Second, we use this to calculate the differential cross section for a dark atom to scatter from a spin singlet to a spin triplet state off of a standard model nucleon and append a form factor to account for recoil of the entire nucleus. Third, we rewrite the resulting rate in terms of the nuclear recoil E_R . Finally, we convolve the recoil rate with the dark matter velocity distribution.

3.1 Non-relativistic Interaction Hamiltonian

In order to calculate the scattering cross section for dark atoms off of standard model nuclei we derive the interaction Hamiltonian by taking the non-relativistic limit of the current-current interaction

$$\mathcal{A} = \langle J_D^\mu D_{\mu\nu} J_Y^\nu \rangle, \quad (35)$$

where $D_{\mu\nu}$ is the Coulomb gauge propagator for X . The leading behavior of Eq. (35) is

$$\begin{aligned} \mathcal{A} \simeq & \frac{g_5 \epsilon c_w e}{\vec{q}^2 + M_X^2} \chi_{s'}^\dagger \left[\frac{\vec{\sigma}_e \cdot \vec{p}_e}{m_e} + \frac{\vec{\sigma}_e \cdot \vec{q}}{2m_e} + \frac{\vec{\sigma}_e \cdot \vec{q}}{2m_n} - \frac{\vec{\sigma}_e \cdot \vec{p}_n}{m_n} + \frac{\vec{\sigma}_p \cdot \vec{p}_n}{m_n} - \frac{\vec{\sigma}_p \cdot \vec{q}}{2m_n} \right. \\ & \left. + \frac{(\vec{\sigma}_e \cdot \vec{q})(\vec{q} \cdot \vec{p}_n)}{m_n(\vec{q}^2 + M_X^2)} - \frac{(\vec{\sigma}_e \cdot \vec{q})\vec{q}^2}{2m_n(\vec{q}^2 + M_X^2)} - \frac{(\vec{\sigma}_p \cdot \vec{q})(\vec{q} \cdot \vec{p}_n)}{m_n(\vec{q}^2 + M_X^2)} + \frac{(\vec{\sigma}_p \cdot \vec{q})\vec{q}^2}{2m_n(\vec{q}^2 + M_X^2)} \right] \chi_s \xi_{r'}^\dagger \xi_r. \end{aligned} \quad (36)$$

where m_n is the nucleon mass, \vec{p}_e is the initial momentum of the dark electron, that of the nucleon is \vec{p}_n and \vec{q} is the momentum conjugate to the relative coordinate between the electron and nucleon. χ_s and $\chi_{s'}$ are the initial and final spin states of the atom and can be written in the form: $\chi_{Atom} = \chi_{\mathbf{p}} \otimes \chi_e$. The dark matter spin operators are $\vec{S}_{e,p} = \mathbb{1} \otimes \vec{\sigma}_e/2, \vec{\sigma}_p/2 \otimes \mathbb{1}$. ξ_r and $\xi_{r'}$ are the initial and final spin states of the standard model nucleon. In the following analysis we consider proton masses of $\mathcal{O}(100 \text{ GeV})$ and electron masses of $\mathcal{O}(1 \text{ GeV})$, so we have ignored terms suppressed by $m_{\mathbf{p}}$. We have also dropped terms suppressed by M_Z . Finally, we have omitted terms which depend on the spin of the standard model nucleon, as we expect these terms to contribute *incoherently* to the overall scattering cross section and hence be suppressed by the atomic number of the nucleus.

3.2 Inelastic Dark Atom - Nucleus Scattering

The cross section in the center of mass of the hydrogen-nucleus system is given by [39, 40]

$$\frac{d\sigma_{hf}}{d\Omega} \equiv \frac{d\sigma}{d\Omega}(S=0 \rightarrow S=1) = \frac{\mu_{NA}^2}{4\pi^2} \left| \frac{k'}{k} \right| \left| \langle \mathbf{p}'_{\mathbf{H}}, \mathbf{p}'_N, N', H' | \hat{H}_{int} | \mathbf{p}_{\mathbf{H}}, \mathbf{p}_N, N, H \rangle \right|^2. \quad (37)$$

Here \hat{H}_{int} is the interaction Hamiltonian, which is obtained from Eq. (36) by Fourier transforming \vec{q} to position space. The prefactor contains $\mu_{NA} \equiv (m_{\mathbf{H}} + M_N)/(m_{\mathbf{H}} + M_N)$ which is the reduced mass of hydrogen and the nucleus, and the momenta \vec{k} and \vec{k}' which are the initial and final momenta conjugate to the relative coordinate between the atom and the nucleus. Our basis is the hydrogen atom momentum $\{\mathbf{p}_{\mathbf{H}}, \mathbf{p}'_{\mathbf{H}}\}$, the nucleus momentum, $\{\mathbf{p}_N, \mathbf{p}'_N\}$, and the internal states of hydrogen and the nucleus, $\{A, A'\}$ and $\{N, N'\}$. The explicit evaluation of the matrix element in Eq. (37) is complicated by the fact

that there are four particles in the incoming and outgoing states. The hydrogen atom and the nucleus are both free particles while the electron and nucleon are bound the respective free particle motion. Since the scattering centers, the electron and nucleon, do not correspond to the coordinates of free particle motion, hydrogen's center of mass and the nucleus's center of mass, the matrix element in Eq. (37) contains an atomic form-factor in addition to the usual nuclear form factor. We find, ignoring terms suppressed by $m_e/m_{\mathbf{H}}$ and m_n/M_N , the cross section to be

$$\begin{aligned} \frac{d\sigma_{hf}}{d\Omega} &= \left| \frac{k'}{k} \right| \left(\frac{2\mu_{NA}^2}{\pi^2} \right) \left(\frac{g_5 Ze \epsilon c_w}{q^2 + M_X^2} \right)^2 \left| \chi_{s'} \right| \left[F_{el}(q^2) \frac{\vec{S}_e \cdot \vec{q}}{\mu_{ne}} - F_{el}(q^2) \frac{(2\vec{S}_e \cdot \vec{q}) q^2}{m_n (q^2 + M_X^2)} \right. \\ &\quad \left. - \frac{\vec{S}_p \cdot \vec{q}}{m_n} + \frac{(2\vec{S}_p \cdot \vec{q}) q^2}{m_n (q^2 + M_X^2)} \right] \chi_s \left| F_{\mathbf{H}}(q^2) \right|^2. \end{aligned} \quad (38)$$

The electron form factor $F_{el}(q^2)$ is found to be

$$F_{el}(q^2) = \langle 0 | e^{i\vec{q} \cdot \vec{r}_e} | 0 \rangle = \left(1 + \frac{q^2 a_0^2}{4} \right)^{-2} \quad (39)$$

where $|0\rangle$ is the ground state of the dark atom. The function $F_H(q^2)$ is the Helm nuclear form factor which accounts for the overlap between nucleon and *nuclear* states [41, 42]. We have averaged over initial nucleon spin and summed over final nucleon spin. Summing over the final atomic spin states and using Eq. (39) we have

$$\frac{d\sigma_{hf}}{d\Omega} = \frac{M_N^2}{2} \left| \frac{k'}{k} \right| \left(\frac{g_5 Ze \epsilon c_w}{\pi} \right)^2 \left(\frac{F_{el} F_H G(q^2)}{M_X^2 \left(1 + \frac{q^2}{M_X^2} \right)} \right)^2 \left(\frac{q}{\mu_{ne}} \right)^2; \quad (40)$$

we have defined the function $G(q^2)$ as follows

$$G(q^2) \equiv 1 + \frac{\mu_{ne}}{m_n} \left[F_{el}^{-1} - (1 + F_{el}^{-1}) \frac{q^2}{q^2 + M_X^2} \right]. \quad (41)$$

We rewrite the above in the following form

$$\frac{d\sigma_{hf}}{dE_R} = \frac{4Z^2 \alpha}{\mu_{ne}^2 f_{eff}^4} \frac{M_N^2}{v_{rel}^2} \frac{E_R F_H^2 F_{el}^2}{(1 + 2M_N E_R / M_X^2)^2} G^2(E_R) \quad (42)$$

$$f_{eff}^4 \equiv \frac{M_X^4}{2(g_5 \epsilon c_w)^2}, \quad (43)$$

where we have defined the scale f_{eff} for compactness and for comparison to Ref. [18].

3.3 Modulated Nuclear Recoil Rate

The amplitude of the modulated recoil rate at a detector with N_T target nuclei of mass M_N is given by

$$\frac{dR}{dE_R} \equiv \frac{1}{2} N_T \frac{\rho}{m_{DM}} \int_{v_{min}}^{v_{esc}} dv_{rel} v_{rel} f(v_{rel}) \frac{d\sigma_{hf}}{dE_R} \Big|_{January}^{June}, \quad (44)$$

where v_{rel} is the relativity velocity between the dark atom and the nucleus, $\rho = 0.3 \text{ GeV/cm}^3$ is the local dark matter density and we use $v_{esc} = 550 \text{ km/s}$ for the dark matter escape velocity – see Ref. [43]. The lower bound on the velocity integration is the minimum relative velocity that can produce a given recoil energy

$$v_{min} \equiv \sqrt{\frac{1}{2 M_N E_R} \left(\frac{M_N + M_{\mathbf{H}}}{M_{\mathbf{H}}} E_R + E_{hf} \right)}. \quad (45)$$

Following Ref's. [43, 44], the velocity distribution in Eq. (44) is approximated by

$$f(v) = \begin{cases} \frac{1}{N} \left(\frac{1}{\pi v_0^2} \right)^{3/2} e^{-v^2/v_0^2}, & \text{for } v < v_{esc} \\ 0, & \text{for } v \geq v_{esc}. \end{cases} \quad (46)$$

The normalization is

$$N = \text{erf} \left(\frac{v_{esc}}{v_0} \right) - \frac{2}{\sqrt{\pi}} \frac{v_{esc}}{v_0} e^{-(v_{esc}/v_0)^2}, \quad (47)$$

with $v_0 = 220 \text{ km/s}$.

Figure 2 is an example of the modulated count rate at DAMA as defined in Eq. (44) with the data points and reported uncertainties from DAMA and DAMA/LIBRA [5]. We have plotted the modulated spectrum for three choices of the set of parameters ($m_{\mathbf{p}}, m_{\mathbf{e}}, \alpha_D, M_X, g_5$ and ϵ) which satisfy the rather stringent list of constraints enumerated below. Note the linear dependence on E_R and the presence of an atomic form factor in Eq. (42). Although the first term tends to push the peak toward larger values of E_R , the atomic form factor turns off scattering when $qa_0 \sim 1$.

Mixing With The Standard Model: Perhaps the harshest constraints are on the mass of the axial $U(1)$ and its kinetic mixing with the standard model, since the direct detection cross section is roughly proportional to ϵ^2/M_X^4 . The one loop contribution of X to the anomolous magnetic moment of the muon is

$$a_{\mu}^X = \frac{\alpha \epsilon^2}{2\pi} \int_0^1 dz \frac{2m_{\mu}^2 z(1-z)^2}{m_{\mu}^2(1-z)^2 + m_X^2 z}. \quad (48)$$

As discussed in Ref. [45], regardless of how one treats the hadronic contribution to the theoretical prediction of a_{μ} , the X boson's one loop contribution must satisfy

$$a_{\mu}^X \leq 7.4 \times 10^{-9}. \quad (49)$$

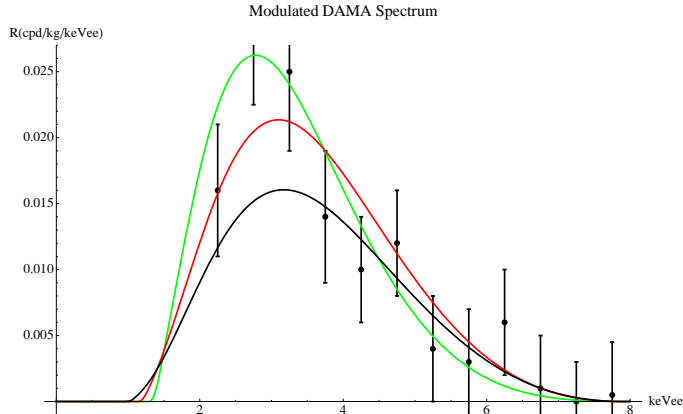


Figure 2: Examples of the modulated spectrum at DAMA defined in Eq. (44) complete with the data points from the DAMA and DAMA/LIBRA experiments. The curves correspond to the following choice of parameters from left to right in order of their rise from zero (black, red and green in color order) $m_p = 200, 100, 70$ GeV; $m_e \simeq 2.1, 1.7, 1.7$ GeV; $f_{eff} \simeq 103, 92, 67$ GeV. The hyperfine splittings are all about 111 keV.

In order to be conservative we restrict ourselves to (see Figure 1 in Ref. [45])

$$M_X \geq 100 \text{ MeV} \text{ and } \epsilon^2 \lesssim 10^{-5}.$$

Mixing between the massless gauge boson in the dark sector and the photon is not induced by loops in our theory, and we nominally set it zero. A constraint on this mixing, ϵ' , can be derived from bounds on its contribution to the anomalous magnetic moment of the electron. The constraint is $\epsilon' < \mathcal{O}(10^{-4})$ [45]. Astrophysical constraints also exist, but are much less restrictive for the range of electron masses we are considering [46].

Sufficient Recombination: The residual ionized dark matter will scatter *elastically* as it does not cost any energy to flip a free spin. Efficient recombination and a hyperfine splitting consistent with DAMA imply that the typical electron mass is $\mathcal{O}(1 \text{ GeV})$ and therefore too small to induce observable nuclear recoils. The strongest constraints on direct detection of the free dark protons come from CDMS [6, 47]. With a net exposure of 174.7 kg-d, the CDMS experiment allows 5.3 signal events at 90% confidence level. To be consistent with the bounds from direct detection⁵ we demand that $X_e \leq 10^{-4}$.

Energy Level Corrections Due to the Axial U(1): The proton-electron interaction due to the broken axial U(1) is a perturbation to the hydrogen Hamiltonian and gives a correction to the hyperfine level splitting. The correction is given by

⁵The discussion in this section actually puts a bound on the *local* ionized fraction. We assume for simplicity – here and throughout the paper – that the distribution of ionized dark matter matches that of atomic dark matter. However, due to the presence of a long-ranged force, it may be that the ionized distribution is very different from the typical dark matter halo. A full N-body simulation of a multiple species halo is beyond the scope of the present work, so for now we ignore this interesting possibility.

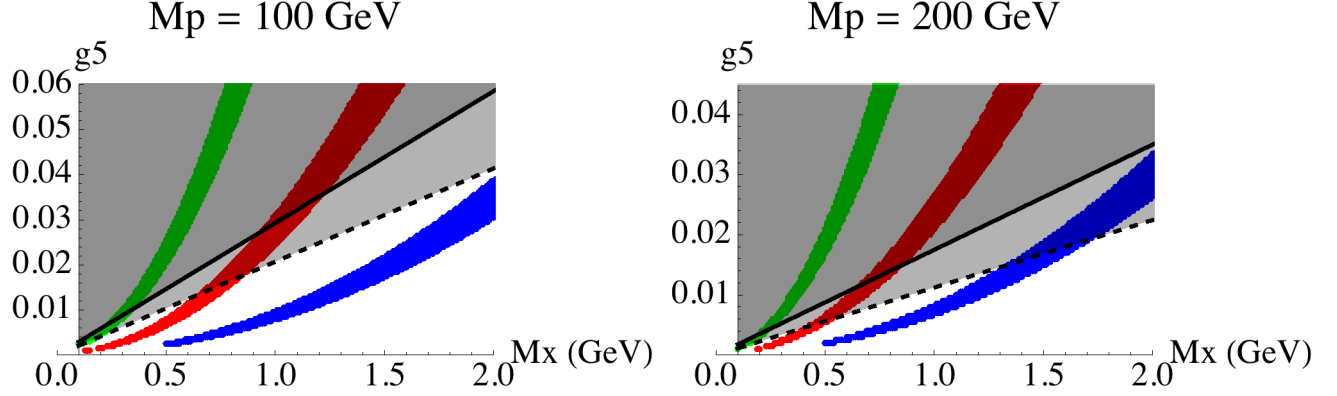


Figure 3: The allowed parameter space for M_X and g_5 for two values of the dark proton mass. The other atomic parameters – α_D and m_e – have been chosen so that $E_{hf} \simeq 111$ keV and $X_e \leq 10^{-4}$. On each plot, the displayed values of ϵ^2 are 10^{-6} , 10^{-5} and 10^{-4} from left to right (green, red and blue in color order). To be consistent with constraints discussed in Ref. [45], $M_X \geq 0.5$ GeV for $\epsilon^2 = 10^{-4}$. The allowed points have an average rate, in the 2 to 6 keVee bins at DAMA, between 0.99×10^{-2} and 1.63×10^{-2} cpd/kg/keVee. The excluded regions correspond to choices of parameters which do not satisfy Eq. (53); the solid black line is for $\Lambda = 1$ TeV and the dashed line is for $\Lambda = 10$ TeV.

$$\delta E_{hf} \sim \langle 0 | \frac{g_5^2 e^{-M_X r}}{4\pi r} | 0 \rangle = \frac{g_5^2}{4\pi a_0} (1 + a_0 M_X)^{-2}. \quad (50)$$

Requiring $\delta E_{hf} \ll E_{hf}$ gives

$$g_5^2 \ll \frac{32\pi}{3} \alpha_D^3 \frac{m_e}{m_{\mathbf{p}}} \left(1 + \frac{M_X}{\alpha_D \mu_H} \right)^2. \quad (51)$$

The parameter sets shown in Figure 2 satisfy this constraint.

Breaking the Axial U(1): Masses for the dark electron, dark proton and the axial gauge boson all violate the axial U(1) symmetry. Perhaps the simplest way to give mass to these particles is giving a vev to a charge +2 scalar ϕ_{+2} , as in [18]

$$\mathcal{L} \ni |D_5^\mu \phi_{+2}|^2 - \lambda \left(|\phi_{+2}|^2 - v_{+2}^2 \right)^2 + y_{\mathbf{p}} (\bar{p}_R \phi_{+2} p_L + \bar{p}_L \phi_{+2}^* p_R) + y_e (\bar{e}_R \phi_{+2} e_L + \bar{e}_L \phi_{+2}^* e_R). \quad (52)$$

When the scalar is at its vev, the mass spectrum is

$$\begin{aligned} M_X &= g_5 v_{+2} \\ m_{\mathbf{p}} &= y_{\mathbf{p}} v_{+2} \\ m_e &= y_e v_{+2}. \end{aligned} \quad (53)$$

The DAMA signal requires $m_{\mathbf{p}} > m_X$ and $g_5 \gtrsim \mathcal{O}(10^{-2})$ thus one might worry about the perturbativity of $y_{\mathbf{p}}$. The yukawa coupling runs according to the following one loop renormalization group evolution [48]

$$y_{\mathbf{p}}(\Lambda) = \sqrt{\frac{2\pi^2}{\ln(\Lambda/m_{\mathbf{p}})}}, \quad (54)$$

which blows up at the scale Λ . If we take $\Lambda = 1$ TeV or 10 TeV, our parameter space is constrained as shown in Figure 3. In principle, the proton could be a composite object and the axial-symmetry breaking could occur at strong coupling (as in QCD) and not via a weakly coupled scalar. The proton could also carry a charge under another gauge interaction that is relatively strong, but breaks at a TeV, thus tempering the UV behavior of y_p . We leave explicit models of UV completions to future work.

Figure 3 displays the allowed parameter space for a few choices of M_X , g_5 and ϵ with $X_e \leq 10^{-4}$ level.

4 Discussion

Dark matter succinctly explains a number of astrophysical and cosmological observations that are otherwise puzzling. Standard WIMP dark matter can accommodate the gross features of these observations and naturally exists in models that attempt to explain the origin of the weak-scale. However, the typical WIMP seems unable to explain observed small-scale structure and tensions between direct detection experiments. These considerations point to the possibility of a non-minimal dark sector, which contains more similarities to the *light sector* than is typically thought. Atomic dark matter – with a non-negligible ionized fraction X_e and a new massless gauge boson – offers the possibility of significantly different phenomena in the dark sector than those of standard WIMPs.

As discussed in Section 2, the residual ionized fraction can keep dark matter in equilibrium with dark radiation long enough to smooth halo structure on small scales. Furthermore, atomic dark matter may have hyperfine transitions of the right size to offer an inelastic explanation for the DAMA data. However, having X_e large enough to smooth out structure is inconsistent with the simultaneous positive DAMA signal and null CDMS signal under the assumption that the charged halo has the same distribution as the atomic halo. Yet, if X_e is large enough, the distribution of the ionized fraction may be smoother and more spherical than standard halo models as suggested in Ref. [49, 50]. If the local ionized dark matter distribution is very different from the atomic dark matter distribution, then parameter space exists which can explain both small-scale structure and the DAMA signal. On the other hand, if our simple model of atomic dark matter is the right explanation for DAMA and the ionized components of the halo follow the distribution of the atomic dark matter, then other direct detection experiments should see dark protons in the near future. Simulations of structure formation with charged and neutral components could shed light on these issues.

The dynamics that lead to atomic dark matter also may have other phenomenological implications. For example, in parts of parameter space where the ionized fraction is large enough, \mathbf{H}_2 molecules may form through processes catalyzed by the residual ions, as in the SM [51]



and



The existence of molecular states in the dark sector offers the possibility of cooling mechanisms which, in the SM, are thought to be very important for the formation of the first stars [52]. This raises the interesting question of whether and to what extent compact objects, *e.g.* dark stars, could form for weak-scale dark atoms. Moreover, if the dark photon mixes with the SM photon, it may result in dark atomic line emissions in cosmic gamma rays.

We have presented a somewhat generic model of atomic dark matter. Explicit models which explain the asymmetry abundance and which serve as ultraviolet completions of the model could potentially relate astrophysical phenomena to physics to be probed by the Large Hadron Collider. The part of parameter space in which the measured DAMA signal is post-dicted requires the dark proton to be strongly coupled, or nearly so, at a TeV. If strongly coupled, one could imagine additional features of the dark sector – *i.e.*, a composite atomic nucleus – which more strongly mimic our visible world.

The authors would like to thank Julian Krolik, Kirill Melnikov, Colin Norman, and Alex Szalay for helpful discussions. This work is supported in part by the National Science Foundation under grant NSF-PHY-0401513, the Department of Energy’s OJI program under grant DE-FG02-03ER4127, and the OWC.

References

- [1] E. Komatsu *et al.* [WMAP Collaboration], *Astrophys. J. Suppl.* **180**, 330 (2009) [arXiv:0803.0547 [astro-ph]].
- [2] K. Abazajian *et al.* [SDSS Collaboration], *Astrophys. J.* **625**, 613 (2005) [arXiv:astro-ph/0408003].
- [3] J. F. Navarro, C. S. Frenk and S. D. M. White, *Astrophys. J.* **462**, 563 (1996) [arXiv:astro-ph/9508025].
- [4] G. Gilmore, M. I. Wilkinson, R. F. G. Wyse, J. T. Kleyana, A. Koch, N. W. Evans and E. K. Grebel, *Astrophys. J.* **663**, 948 (2007) [arXiv:astro-ph/0703308].
- [5] R. Bernabei *et al.* [DAMA Collaboration], *Eur. Phys. J. C* **56**, 333 (2008) [arXiv:0804.2741 [astro-ph]].
- [6] Z. Ahmed *et al.* [CDMS Collaboration], *Phys. Rev. Lett.* **102**, 011301 (2009) [arXiv:0802.3530 [astro-ph]].
- [7] J. Angle *et al.* [XENON Collaboration], *Phys. Rev. Lett.* **100**, 021303 (2008) [arXiv:0706.0039 [astro-ph]].
- [8] O. Adriani *et al.* [PAMELA Collaboration], *Nature* **458**, 607 (2009) [arXiv:0810.4995 [astro-ph]].
- [9] J. Chang *et al.*, *Nature* **456**, 362 (2008).
- [10] S. Torii *et al.* [PPB-BETS Collaboration], arXiv:0809.0760 [astro-ph].
- [11] A. A. Abdo *et al.* [The Fermi LAT Collaboration], *Phys. Rev. Lett.* **102**, 181101 (2009) [arXiv:0905.0025 [astro-ph.HE]].
- [12] C. Amsler *et al.* [Particle Data Group], *Phys. Lett. B* **667**, 1 (2008).

- [13] D. E. Kaplan, M. A. Luty and K. M. Zurek, arXiv:0901.4117 [hep-ph].
- [14] G. R. Farrar and G. Zaharijas, Phys. Rev. Lett. **96**, 041302 (2006) [arXiv:hep-ph/0510079].
- [15] D. Tucker-Smith and N. Weiner, Phys. Rev. D **64**, 043502 (2001) [arXiv:hep-ph/0101138].
- [16] J. L. Feng, M. Kaplinghat, H. Tu and H. B. Yu, arXiv:0905.3039 [hep-ph].
- [17] L. Ackerman, M. R. Buckley, S. M. Carroll and M. Kamionkowski, Phys. Rev. D **79**, 023519 (2009) [arXiv:0810.5126 [hep-ph]].
- [18] D. S. M. Alves, S. R. Behbahani, P. Schuster and J. G. Wacker, arXiv:0903.3945 [hep-ph].
- [19] Z. Berezhiani, arXiv:hep-ph/0508233.
- [20] R. N. Mohapatra, S. Nussinov and V. L. Teplitz, Phys. Rev. D **66**, 063002 (2002) [arXiv:hep-ph/0111381].
- [21] A. A. Klypin, A. V. Kravtsov, O. Valenzuela and F. Prada, Astrophys. J. **522**, 82 (1999) [arXiv:astro-ph/9901240].
- [22] B. Moore, S. Ghigna, F. Governato, G. Lake, T. R. Quinn, J. Stadel and P. Tozzi, Astrophys. J. **524**, L19 (1999).
- [23] P. J. E. Peebles, Astrophys. J. **153**, 1 (1968).
- [24] S. Dodelson, *Modern Cosmology* (Academic Press, San Diego, 2003).
- [25] C. P. Ma and E. Bertschinger, Astrophys. J. **455**, 7 (1995) [arXiv:astro-ph/9506072].
- [26] L. Spitzer 1978, *Physical Processes in the Interstellar Medium*, (Wiley, New York)
- [27] L. J. Spitzer and J. L. Greenstein Astrophys. J. **114**, 407 (1952).
- [28] L. D. Landau and E. M. Lifshitz, *Quantum Mechanics: Non-Relativistic Theory* (Pergamon Press Ltd., London – Paris, 1958.)
- [29] T. Wu and T. Ohmura, *Quantum Theory of Scattering*(Prentice-Hall Inc., New Jersey, 1962.)
- [30] B.H. Bransden and C.J. Joachain, *Physics of Atoms and Molecules*(Addison Wesley Longman Ltd., Essex, 1983.)
- [31] D. R. Schultz, P. S. Krstic, T. G. Lee and L. C. Raymond Astrophys. J. **114**, 407 (1952).
- [32] P. S. Krstic, and D .R. Schultz J. Phys. B **32** 3485 (1999)
- [33] P. S. Krstic, J. H. Macek, S. Yu. Ovchinnikov, and D. R. Schultz Phys. Rev. A **70** 042711 (2004)
- [34] M. Markevitch *et al.*, Astrophys. J. **606**, 819 (2004) [arXiv:astro-ph/0309303].
- [35] S. W. Randall, M. Markevitch, D. Clowe, A. H. Gonzalez and M. Bradac, arXiv:0704.0261 [astro-ph].
- [36] J. Miralda-Escude, arXiv:astro-ph/0002050.

- [37] A. Loeb and M. Zaldarriaga, Phys. Rev. D **71**, 103520 (2005) [arXiv:astro-ph/0504112].
- [38] D. Hooper, M. Kaplinghat, L. E. Strigari and K. M. Zurek, Phys. Rev. D **76**, 103515 (2007) [arXiv:0704.2558 [astro-ph]].
- [39] J. J. Sakurai, *Modern Quantum Mechanics* (Addison-Wesley Publishing Company, 1995), Revised
- [40] R. Shankar, *Principles of Quantum Mechanics* (Springer, 1994)
- [41] R. H. Helm, Phys. Rev. **104**, 1466 (1956).
- [42] G. Jungman, M. Kamionkowski and K. Griest, Phys. Rept. **267**, 195 (1996) [arXiv:hep-ph/9506380].
- [43] J. D. Lewin and P. F. Smith, Astropart. Phys. **6**, 87 (1996).
- [44] C. Savage, K. Freese and P. Gondolo, Phys. Rev. D **74**, 043531 (2006) [arXiv:astro-ph/0607121].
- [45] M. Pospelov, arXiv:0811.1030 [hep-ph].
- [46] S. Davidson, S. Hannestad and G. Raffelt, JHEP **0005**, 003 (2000) [arXiv:hep-ph/0001179].
- [47] S. Chang, G. D. Kribs, D. Tucker-Smith and N. Weiner, Phys. Rev. D **79**, 043513 (2009) [arXiv:0807.2250 [hep-ph]].
- [48] M. E. Machacek and M. T. Vaughn, Nucl. Phys. B **236**, 221 (1984).
- [49] B. D. Wandelt, R. Dave, G. R. Farrar, P. C. McGuire, D. N. Spergel and P. J. Steinhardt, arXiv:astro-ph/0006344.
- [50] R. Dave, D. N. Spergel, P. J. Steinhardt and B. D. Wandelt, Astrophys. J. **547**, 574 (2001) [arXiv:astro-ph/0006218].
- [51] C. M. Hirata and N. Padmanabhan, Mon. Not. Roy. Astron. Soc. **372**, 1175 (2006) [arXiv:astro-ph/0606437].
- [52] N. Yoshida, K. Omukai, L. Hernquist and T. Abel, Astrophys. J. **652**, 6 (2006) [arXiv:astro-ph/0606106].